Human Pathology (2019) **86**, 38–48

ELSEVIER

Human PATHOLOGY

www.elsevier.com/locate/humpath

Original contribution

Molecular features of pleomorphic xanthoastrocytoma☆,☆☆

Han Zou MD[a,b], Yumei Duan MA[c], Dongliang Wei MA[d], Yiqian Zhang MD[a], Jiacheng Dai MA[e], Junzhi Li MA[f], Xiaojie Li MA[g], Jianhua Zhou MD[c,h], Zhixiong Liu MD[b], Zhongyuan Jin MD[c,h], Zhou Zhang PhD[i], Yang Yu MD[a], Zhongliang Hu MD PhD[c,h,j,*]

[a]*Department of Eight-Grade Clinical Medicine, Xiangya Medical School, Central South University, Changsha 410008, China*
[b]*Department of Neurosurgery, Xiangya Hospital, Central South University, Changsha 410008, China*
[c]*Department of Pathology, Xiangya Hospital, Central South University, Changsha 410008, China*
[d]*Xiangya School of Stomatology, Central South University, Changsha 410000, China*
[e]*Center for Medical Genetics, School of Life Sciences, Central South University, Changsha 410078, China*
[f]*Department of Pathology, The First Affiliated Hospital of Xinjiang Medical University, Xinjiang Medical University, Urumqi 830054, China*
[g]*Department of Pathology, the First People's Hospital of Chenzhou, Chenzhou 423000, China*
[h]*Department of Pathology, Xiangya Medical School, Central South University, Changsha 410013, China*
[i]*Burning Rock Biotech, Guangzhou 510300, China*
[j]*Department of Pathology, Institute of Basic Medicine, Xinjiang Medical University, Urumqi 830011, China*

Received 6 June 2018; revised 23 August 2018; accepted 29 August 2018

Keywords:
MAPK pathway;
Next-generation sequencing;
Pleomorphic xanthoastrocytoma;
Molecular feature;
Microsatellite stability

Summary Pleomorphic xanthoastrocytoma (PXA) is a rare central nervous system tumor occurring mostly in children and young adults. Next-generation sequencing of 295 cancer-related genes was used to investigate the molecular profiles of 13 cases of PXA. We found that *BRAF* V600E (5/13; 38%), *FANCA/D2/I/M* (5/13; 38%), *PRKDC* (4/13; 31%), *NF1* (3/13; 23%), and *NOTCH2/3/4* (3/13; 23%) alterations were the most frequent somatic gene mutations. However, neither *PTEN* nor *EGFR* mutation, which is frequently present in glioblastoma, was detected. The *KRAS* mutation in PXA is reported for the first time in these tumors. Microsatellite stability was present in all cases. Because mutations of *FANCA* and *BRAF* and copy number variations of *CDKN2A/B* are more frequent in PXA than in glioblastoma, they might be used to distinguish the 2 tumors. The MAPK pathway is involved in the pathogenesis of PXA and may be an effective target for treatment.

1. Introduction

Although it has been almost 40 years since pleomorphic xanthoastrocytoma (PXA) was first described by Kepes and associates [1], our understanding of the tumor has been limited by its rarity [2].

☆ Competing interests: The authors declare no conflicts of interest.
☆☆ Funding/Support: This work was supported by the Undergraduate Free Exploration Program of Central South University (Grant No. ZY2016715) and the Undergraduate Innovation Training Program of Central South University (Grant No. CX20170481).
* Corresponding author at: Department of Pathology, Xiangya Hospital, Central South University, Changsha 410000, Hunan Province, China.
E-mail address: huzhongliang@csu.edu.cn (Z. Hu).

https://doi.org/10.1016/j.humpath.2018.08.038
0046-8177/

It is noteworthy that although PXA and epithelioid glioblastoma multiforme (GBM) demonstrate similar morphologic and partially similar molecular features, such as wild-type *IDH1* and *MGMT* promoter hypermethylation [3], the tumors have a totally different prognosis. Therefore, it is necessary to differentiate PXA from epithelioid GBM to avoid overtreatment. There is at present no reliable biomarker to distinguish PXA from GBM.

Although there are several studies on the molecular characteristics of PXA, it has not been fully explored. Next-generation sequencing (NGS) was performed in our study to gain a better understanding of PXA's molecular profile. Mutations in *BRAF* V600E, *FANCA/D2/I/M*, *PRKDC*, *NF1*, and *NOTCH2/3/4* were the most frequent somatic mutations in our patients with PXA. Moreover, *KRAS* mutations are reported for the first time.

2. Materials and methods

2.1. Patient samples

This study was approved by the institutional review boards of Xiangya Hospital affiliated with Central South University, The First Affiliated Hospital of Xinjiang Medical University, and The First People's Hospital of Chenzhou. The cases of PXA, consisting of 10 from Xiangya Hospital, 1 from The First Affiliated Hospital of Xinjiang Medical University, and 2 from The First People's Hospital of Chenzhou, were confirmed by 2 neuropathologists according to the latest (2016 edition) World Health Organization (WHO) classification of tumors of the central nervous system [2]. None of the 13 patients had anaplastic PXA, so such lesions were unavailable for our study. Clinical data including patient sex, age, tumor site and clinical manifestation, and immunohistologic features were collected. Specimen blocks from the 13 lesions were obtained by surgery without prior treatment with radiation or chemotherapy and were sent to Burning Rock Biotech, Inc (Guangzhou, China) for NGS, which is certified by the Clinical Laboratory Improvement Amendments (OncoScreen).

2.2. DNA extraction

Five to eight 10-μm tissue sections from formalin-fixed, paraffin-embedded (FFPE) tumor samples and adjacent normal tissue were collected for the genetic analysis. A parallel hematoxylin and eosinE); slide was used as a reference to make sure that the neoplastic area was microdissected precisely. The DNA from samples with >80% tumor tissue was isolated and extracted with the QIAamp DNA FFPE Tissue Kit (Qiagen, Heidelberg, Germany). The DNA quality was evaluated by NanoDrop 8000 (ThermoFisher Scientific, Waltham, MA), and the quantity was measured by Qubit dsDNA HS Assay Kit (Invitrogen, Carlsbad, CA) on a Qubit 3.0 Fluorometer.

2.3. NGS library preparation and capture-based targeted sequencing

The capture-based targeted sequencing panel (Burning Rock Biotech) includes missense, synonymous, deletion, amplification, splice, frameshift, and nonsense mutations of all the exons of 295 genes frequently rearranged in cancer and all the introns in 22 cancer-related genes (Supplementary Table). The DNA shearing, end repair, and adaptor ligation were performed using Covaris M220 (Covaris, Waltham, MA). Fragments with sizes between 200 and 400 bp were selected by Agencourt AMPure beads (Beckman Coulter, Atlanta, GA) followed by hybridization with capture probe baits, hybrid selection with magnetic beads, and polymerase chain reaction amplification. Subsequently, the quality and size of the fragments were assessed by Qubit 3.0 and Agilent 2100 bioanalyzer (Agilent Technologies, Santa Clara, CA). With pair-end reads, indexed samples were sequenced on Nextseq500 sequencer (Illumina, San Diego, CA).

2.4. Sequencing data analysis

Sequencing data were mapped to the human genome (hg19) using BWA aligner 0.7.10. Employing GATK 3.2, MuTect, and VarScan, local alignment optimization, variant calling, and annotation were completed. Variants whose depth was less than 100 were filtered out using the VarScan fpfilter pipeline. A minimum of 5 supporting reads were needed for INDELs, and 8 were needed for SNV calling. Variants with a population frequency exceeding 0.1% were grouped as single nucleotide polymorphisms (SNPs) and excluded from further analysis according to the ExAC, 1000 Genomes, dbSNP, and ESP6500SI-V2 databases. Finally, the remaining variants were annotated using ANNOVAR and SnpEff v. 3.6, and DNA translocation analysis was performed with both Tophat2 and Factera 1.4.3. The degree of germline mutation was divided into "pathogenic," "likely pathogenic," "uncertain significance," "likely benign," and "benign" according to ACMG [4].

2.5. Immunohistochemistry

The FFPE tissue sections were used for immunohistochemistry staining, as described previously [4]. In brief, the slides of the lesions from the 13 patients were incubated with primary antibody against GFAP (rabbit monoclonal, clone EP13; ZSGB-Bio, Bejing, China), Ki-67 (mouse monoclonal, clone UMAB107; ZSGB-Bio), p53 (mouse monoclonal, clone DO-7; Fuzhou Maixin Biotech, Fuzhou, China), MGMT (mouse monoclonal, clone UMAB56; ZSGB-Bio), IDH1 (mouse monoclonal, clone H09; ZSGB-Bio), PMS2 (mouse monoclonal, clone MOR4G; Fuzhou Maixin Biotech), MLH1 (mouse monoclonal, clone ES05; ZSGB-Bio), MSH6 (mouse monoclonal, clone 44; Fuzhou Maixin Biotech), and MSH2 (rabbit monoclonal, clone RED2; ZSGB-Bio).

Antibody staining was performed by diaminobenzidine tetrahydrochloride peroxidase substrate solution (Fuzhou Maixin Biotech). Cell nuclei were counterstained with hematoxylin QS (Vector Laboratories, Burlingame, CA). Immunoglobulin G (IgG) was used as a negative control.

2.6. Gene ontology enrichment analysis

Gene ontology (GO) enrichment analysis was carried out with Metascape (http://metascape.org) [5]. Biological process, cellular components, and molecular function of the 61 genes were analyzed following GO biological processes, cellular components, and molecular functions. All genes in the genome were used as the enrichment background. Terms with a .;$P < .005$, minimum count of 3, and enrichment factor >1.5 (enrichment factor is the ratio between observed count and the count expected by chance) are collected and grouped into clusters based on their membership similarities. More specifically, P values are calculated on the basis of accumulative hypergeometric distribution, and q values are calculated using the Banjamini-Hochberg procedure to account for multiple testing. κ scores were used as the similarity metric when performing hierarchical clustering on the enriched terms, and subtrees with a similarity >0.3 were considered a cluster. The most statistically significant term within a cluster was chosen as the one representing the cluster.

2.7. Protein-protein interaction enrichment analysis

With the help of Metascape [5], protein-protein interaction enrichment analysis was carried out with BioGrid, InWeb_IM, and OmniPath. The resultant network contained the subset of proteins that exhibit physical interactions with at least one other list member. If the network contains 3 to 500 proteins, the Molecular Complex Detection (MCODE) algorithm was applied to identify densely connected network components.

2.8. Statistical analysis

Clinical characteristics were compared in patients with and without mutations using the χ^2 or Fisher' exact test. In 12 patients, the germline mutations were compared in pediatric (≤18 years) and adult (>18) patients. All analyses were performed using SPSS version 18 (SPSS, Chicago, IL). A $P < .005$ was considered statistically significant [6].

3. Results

3.1. Clinical and histopathologic features

As shown in Table 1, male patients were more often affected than female patients, with a male-to-female ratio of

Table 1 Clinical and immunohistochemical features of PXA

Case	Sex	Age (y)	Site	Clinical manifestations	Immunohistochemistry
1	M	15	Suprasellar region	Vertigo, fatigue, and memory deterioration for 5 mo	GFAP+, Olig2+, Ki-67 (1%+), p53+, MGMT−, IDH1−, MLH1+, PMS2+, MSH2+, MSH6+
2	F	27	Left medulla oblongata	Seizures, headache, and vomiting for 1 wk	GFAP+, Olig2+, Ki-67 (<1%+), p53−, MGMT−, IDH1−, MLH1+, PMS2+, MSH2+, MSH6+
3	M	50	Cervical spinal cord	Increased numbness of left leg for 2 mo and right leg numbness for 10 d	GFAP+, Olig2+, Ki-67 (2%+), p53+, MGMT−, IDH1−, MLH1+, PMS2+, MSH2+, MSH6+
4	M	5	Right parietal lobe	Seizures for 2 d	GFAP+, Olig2+, Ki-67 (2%+), p53+, MGMT−, IDH1−, MLH1+, PMS2+, MSH2+, MSH6+
5	M	9	Right temporal lobe	Seizures for 1 mo	GFAP+, Olig2 (++), Ki-67 (1%+), p53+, MGMT+, IDH1−, MLH1 (weakly +), PMS2 (weakly +), MSH2+, MSH6+
6	F	25	Left frontal lobe	Seizures for 14 y	GFAP+, Olig2+, Ki-67 (<1%+), p53−, MGMT−, IDH1−, MLH1+, PMS2+, MSH2+, MSH6+
7	M	10	Right temporal lobe	Headache, dizziness, and seizures for 8 mo	GFAP+, Olig2+, Ki-67−, p53 (interspersed +), MGMT−, IDH1−, MLH1+, PMS2+, MSH2+, MSH6+
8	M	8	Left parietal lobe	Seizures for 3 mo	GFAP+, Olig2+, Ki-67 (5%+), p53−, MGMT−, IDH1−, MLH1+, PMS2+, MSH2+, MSH6+
9	F	12	Right frontal lobe	Headache for 20 d	GFAP+, Olig2+, Ki-67 (3%+), p53−, MGMT−, IDH1−, MLH1+, PMS2+, MSH2+, MSH6+
10	F	29	Right cerebellum	Nausea for 6 mo, headache and vomiting for 2 mo	GFAP+, Olig2+, Ki-67 (1%+), p53−, MGMT−, IDH1−, MLH1+, PMS2+, MSH2+, MSH6+
11	M	49	Right occipital lobe	Seizures for 3 mo	GFAP+, Olig2+, Ki-67 (6−8%), p53−, MGMT−, IDH1−, MLH1+, PMS2+, MSH2+, MSH6+
12	M	17	Right parietal lobe	Dizziness and headache for 10 d and vomiting for 2 d	GFAP+, Olig2+, Ki-67 (7%+), p53−, MGMT−, IDH1−, MLH1+, PMS2+, MSH2+, MSH6+
13	M	12	Right temporal lobe	Seizures for 1 d	GFAP+, Olig2+, Ki-67 (5%+), p53−, MGMT−, IDH1−, MLH1+, PMS2+, MSH2+, MSH6+

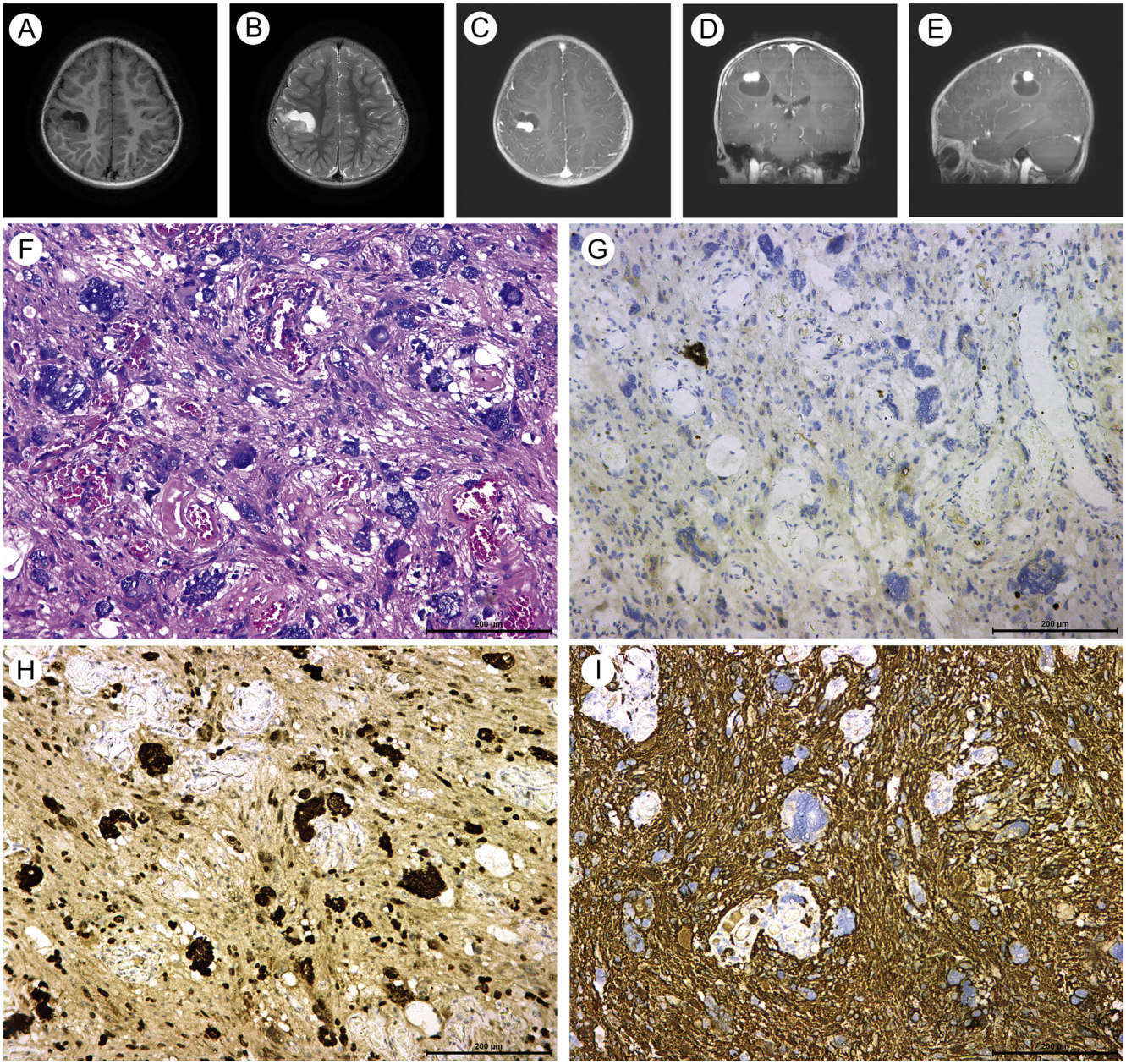

Fig. 1 Magnetic resonance and histologic features of PXA. Magnetic resonance images of PXA in the right parietal lobe showing T_1-weighted (A), T_2-weighted (B), cross-sectional–enhanced (C), coronal plane–enhanced (D), and sagittal plane–enhanced images (E). F, Pleomorphic giant tumor cells with accumulation of lipid in cytoplasm (hematoxylin and eosin stain). Immunohistochemistry staining of Ki-67 (G), Olig2 (H), and GFAP (I). F-I, Scale bar, 200 µm.

2.25. The mean patient age at diagnosis was 20.6 years, ranging from 5 to 50 years. Eight patients (61.5%) were younger than 18 years. All of the neoplasms were primary resection specimens, corresponding histologically to WHO grade II. As shown in Fig. 1, PXA generally was a superficial cystic mass with strong contrast enhancement in its solid component. Tumor cells showed nuclear and cytoplasmic pleomorphism and xanthomatous changes with accumulation of lipids in the cytoplasm. Immunoreactivities for both GFAP and Olig2 demonstrated the essential nature of PXA as a glial tumor (Fig. 1).

3.2. Somatic mutations in PXA

As shown in Fig. 2, 80 genomic alterations (GAs) were detected in the cohort, with an average of 6 GAs, ranging from 1 to 14 GAs, per patient. In total, mutations were present in 61 genes. The most frequently mutated genes were *BRAF* V600E (n = 5; 38%), *FANCA/D2/I/M* (n = 5; 38%), *PRKDC* (n = 4; 31%), *NF1* (n = 3; 23%), and *NOTCH2/3/4* (n = 3). In detail, the mutation rates in *FANCA/D2/I/M* were 23% (E63V, C69S, and Q1437K), 8%

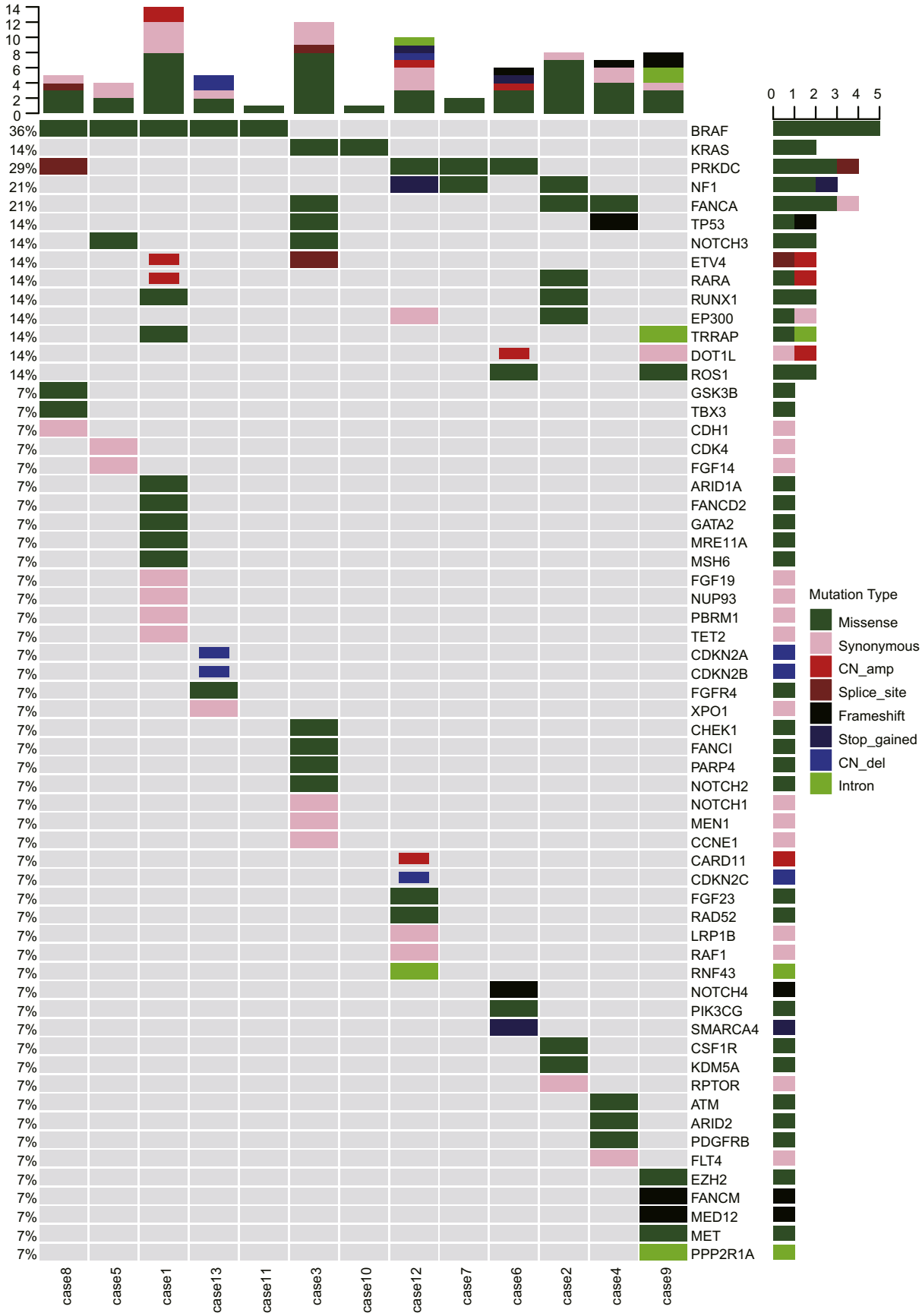

Fig. 2 Summary of DNA mutations and copy numbers in PXA.

Table 2 Summary of mutation types, abundance, mutation sites, copy number variations, alternative nucleotides, and amino acids

Case	Gene	Mutation (variant)	Exon rank	Description	COSM_ID	VAF (%)	Chromosome	Position	Ref	Alt
1	*BRAF*	Missense	15	V600E	COSM476	31	7	1.4×10^8	A	T
	ARID1A	Missense	20	L2195F	NA	66	1	27 106 972	C	T
	FGF19	Synonymous	1	I42	NA	42.50	11	69 518 519	G	A
	MRE11A	Missense	9	M297T	NA	48.90	11	94 203 773	A	G
	NUP93	Synonymous	12	Q443	NA	29.50	16	56 866 284	G	A
	MSH6	Missense	9	K1315T	NA	44.30	2	48 033 733	A	C
	MSH6	Missense	9	E1322D	NA	45.60	2	48 033 755	A	T
	RUNX1	Missense	9	E422A	NA	3.10	21	36 164 610	T	G
	FANCD2	Missense	43	P1468S	NA	49.20	3	10 140 620	C	T
	PBRM1	Synonymous	16	P741	NA	70.70	3	52 643 673	C	T
	GATA2	Missense	3	G94D	NA	58.70	3	1.28×10^8	C	T
	TET2	Synonymous	11	P1601	NA	43.60	4	1.06×10^8	A	C
	TRRAP	Missense	41	M1985I	NA	30	7	98 553 807	G	A
	ETV4	CN amp	NA	4.8	NA	NA	17q21.31	17q21.31	NA	NA
	RARA	CN amp	NA	19.88	NA	NA	17q21.2	17q21.2	NA	NA
2	*KDM5A*	Missense	28	K1680E	NA	44	12	394 657	T	C
	FANCA	Missense	3	C69S	NA	32.40	16	89 881 006	A	T
	NF1	Missense	37	F1613L	NA	61.50	17	29 652 841	C	G
	NF1	Missense	37	I1679M	NA	37.20	17	29 653 039	C	G
	NF1	Missense	37	F1740L	NA	43.60	17	29 653 222	C	A
	NF1	Missense	37	S1754C	NA	34.90	17	29 653 263	C	G
	RARA	Missense	8	P456R	NA	50	17	38 512 408	C	G
	RPTOR	Synonymous	24	T957	NA	32.80	17	78 899 232	G	C
	RUNX1	Missense	9	E422A	NA	4.24	21	36 164 610	T	G
	EP300	Missense	8	M556V	NA	62.10	22	41 533 700	A	G
	CSF1R	Missense	17	G747V	NA	38.90	5	1.49×10^8	C	A
3	*NOTCH2*	Missense	34	R2298W	NA	54.60	1	1.2×10^8	G	A
	MEN1	Synonymous	4	G219	NA	54.20	11	64 575 375	A	G
	CHEK1	Missense	8	P318A	NA	45.30	11	1.26×10^8	C	G
	KRAS	Missense	3	Q61H	COSM1135364, COSM554	46	12	25 380 275	T	G
	PARP4	Missense	12	L482F	NA	36.90	13	25 058 795	G	A
	FANCI	Missense	36	L1253V	NA	56	15	89 857 879	C	G
	FANCA	Missense	43	Q1437K	NA	51.90	16	89 805 068	G	T
	TP53	Missense	7	R248Q	COSM3356964,COSM99021, COSM1640830,COSM10662, COSM99602,COSM99020	53	17	7 577 538	C	T
	ETV4	Splice acceptor	7	NA	NA	54.10	17	41 610 718	T	C
	NOTCH3	Missense	27	R1666W	NA	53	19	15 281 260	G	A
	CCNE1	Synonymous	10	I298	NA	45.60	19	30 313 200	A	C
	NOTCH1	Synonymous	8	N454	NA	49.80	9	1.39×10^8	G	A
4	*ATM*	Missense	48	Y2281H	NA	46	11	1.08×10^8	T	C
	ARID2	Missense	15	R1464C	NA	52.50	12	46 246 296	C	T
	FANCA	Synonymous	42	R1409	NA	54.20	16	89 805 323	C	T
	FANCA	Missense	2	E63V	NA	48.40	16	89 882 286	T	A
	PDGFRB	Missense	15	P727H	NA	50.80	5	1.5×10^8	G	T
	FLT4	Synonymous	29	S1295	NA	44	5	1.8×10^8	G	A
	TP53	Frameshift	5	Y163	COSM45810	3.23	17	7 578 440	TG	T
5	*CDK4*	Synonymous	5	S199=	NA	56.50	12	58 144 474	A	G
	FGF14	Synonymous	1	V5=	NA	61.60	13	1.03×10^8	C	A
	NOTCH3	Missense	11	R607H	NA	42.50	19	15 297 936	C	T
	BRAF	Missense	15	V600E	COSM476	60.10	7	1.4×10^8	A	T
6	*SMARCA4*	Stop gained	20	R978	COSM1266239, COSM1266240	54.70	19	11 134 266	C	T
	ROS1	Missense	32	S1765R	NA	39.50	6	1.18×10^8	A	C
	PIK3CG	Missense	2	V352M	COSM252718	44.10	7	1.07×10^8	G	A

Table 2 (*continued*)

Case	Gene	Mutation (variant)	Exon rank	Description	COSM_ID	VAF (%)	Chromosome	Position	Ref	Alt
	PRKDC	Missense	65	S2997P	NA	42.40	8	48 734 284	A	G
	NOTCH4	Frameshift	1	C17fs	NA	3.80	6	32 191 658	T	AGGCTG
	DOT1L	CN amp	NA	CN amp	NA	3.27	19p13.3	19p13.3	48	29
7	*NF1*	Missense	4	N151S	NA	52.00	17	29 490 367	A	G
	PRKDC	Missense	60	R2728C	NA	62.80	8	48 744 455	G	A
8	*BRAF*	Missense	15	V600E	COSM476	29.10	7	1.4×10^8	A	T
	TBX3	Missense	1	P22L	NA	52.00	12	1.15×10^8	G	A
	CDH1	Synonymous	14	G760=	COSM972802	48.40	16	68 862 192	C	T
	GSK3B	Missense	5	I182V	NA	49.80	3	1.2×10^8	T	C
	PRKDC	Splice region	71	D3307V	NA	50.80	8	48 713 547	T	A
9	*FANCM*	Frameshift	11	K610 fs	NA	54.07	14	45 636 184	G	GTA
	DOT1L	Synonymous	14	P426=	NA	47.50	19	2 210 781	C	G
	PPP2R1A	Intron	4	c.271-15G>A	NA	46.95	19	52 714 498	G	A
	ROS1	Missense	24	I1276T	NA	44.02	6	1.18×10^8	A	G
	TRRAP	Intron	26	c.3852+10C>G	NA	40.55	7	98 529 298	C	G
	MET	Missense	2	N371K	NA	49.41	7	1.16×10^8	C	A
	EZH2	Missense	16	C647S	NA	42.19	7	1.49×10^8	C	G
	MED12	Frameshift	12	L558 fs	NA	7.38	X	70 343 495	TC	T
10	*KRAS*	Missense	3	Q61K	NA	29.18	12	25 380 277	GA	TT
11	*BRAF*	Missense	15	V600E	COSM476	18.99	7	1.4×10^8	A	T
12	*RAD52*	Missense	6	A154T	NA	49.20	12	1 036 318	C	T
	FGF23	Missense	1	A45D	NA	42.00	12	4 488 615	G	T
	NF1	Stop gained	12	R461	COSM24464,COSM977404	81.72	17	29 533 378	C	T
	RNF43	Intron	4	c.450+19G>A	NA	11.42	17	56 440 868	C	T
	CDKN2C	CN del	NA	CN del	NA	0.96	1p32.3	1p32.3	2	1
	LRP1B	Synonymous	43	L2349=	NA	19.25	2	1.41×10^8	C	G
	EP300	Synonymous	14	P802=	NA	28.07	22	41 545 791	G	A
	RAF1	Synonymous	4	A110=	NA	18.71	3	12 650 825	T	C
	CARD11	CN amp	NA	CN amp	NA	3.32	7p22.2	7p22.2	24	14
	PRKDC	Missense	46	T2062I	NA	18.25	8	48 772 191	G	A
13	*XPO1*	Synonymous	14	G506=	NA	48.65	2	61 719 750	T	C
	FGFR4	Missense	5	T167 N	NA	47.01	5	1.77×10^8	C	A
	BRAF	Missense	15	V600E	COSM476	37.29	7	1.4×10^8	A	T
	CDKN2A	CN del	NA	CN del	NA	0.65	9p21.3	9p21.3	5	5
	CDKN2B	CN del	NA	CN del	NA	0.56	9p21.3	9p21.3	2	2

Abbreviations: amp, amplification; Alt, alteration; CN, copy number; del, deletion; NA, not available; Ref, reference; VAF, variant allele frequency.

(P1468S), 8% (L1253 V), and frameshift, respectively (Fig. 2 and Table 2).

Besides the missense mutations, copy number variations were present in 4 patients (cases 1, 6, 12, and 13), including amplifications of *ETV4* and *RARA* in case 1, *DOT1L* amplification in case 6, amplification of *CARD11* and deletion of *CDKN2C* in case 12, and deletion of *CDKN2A* and *CDKN2B* in case 13. Moreover, splice variants were detected in *ETV4* (case 3) and *PRKDC* (case 8). Both copy number amplification and splice variants in *ETV4* were detected in case 3, with frameshift mutations of *FANCM* and *MED12* in case 9 and frameshift mutations of *NOTCH4* and *TP53* in case 4. In addition, nonsense mutations of *SMARCA4* in case 6 and *NF1* in case 12 were identified. It is noteworthy that a *KRAS* mutation was detected for the first time in 2 of our patients, which were mutually exclusive to a *BRAF* V600E mutation. The *KRAS* mutation was present in the 61st codon as *Q61K* and *Q61H*, which is the common mutated codon in other tumors. Interestingly, MAPK pathway–related mutant genes were detected in all 13 patients.

3.3. Germline mutations in PXA

Twelve PXA cases were analyzed for germline mutation and displayed 3307 mutations, with 76 (2.3%) of uncertain significance, 60 (1.8%) likely benign, and 3171 (95.9%)

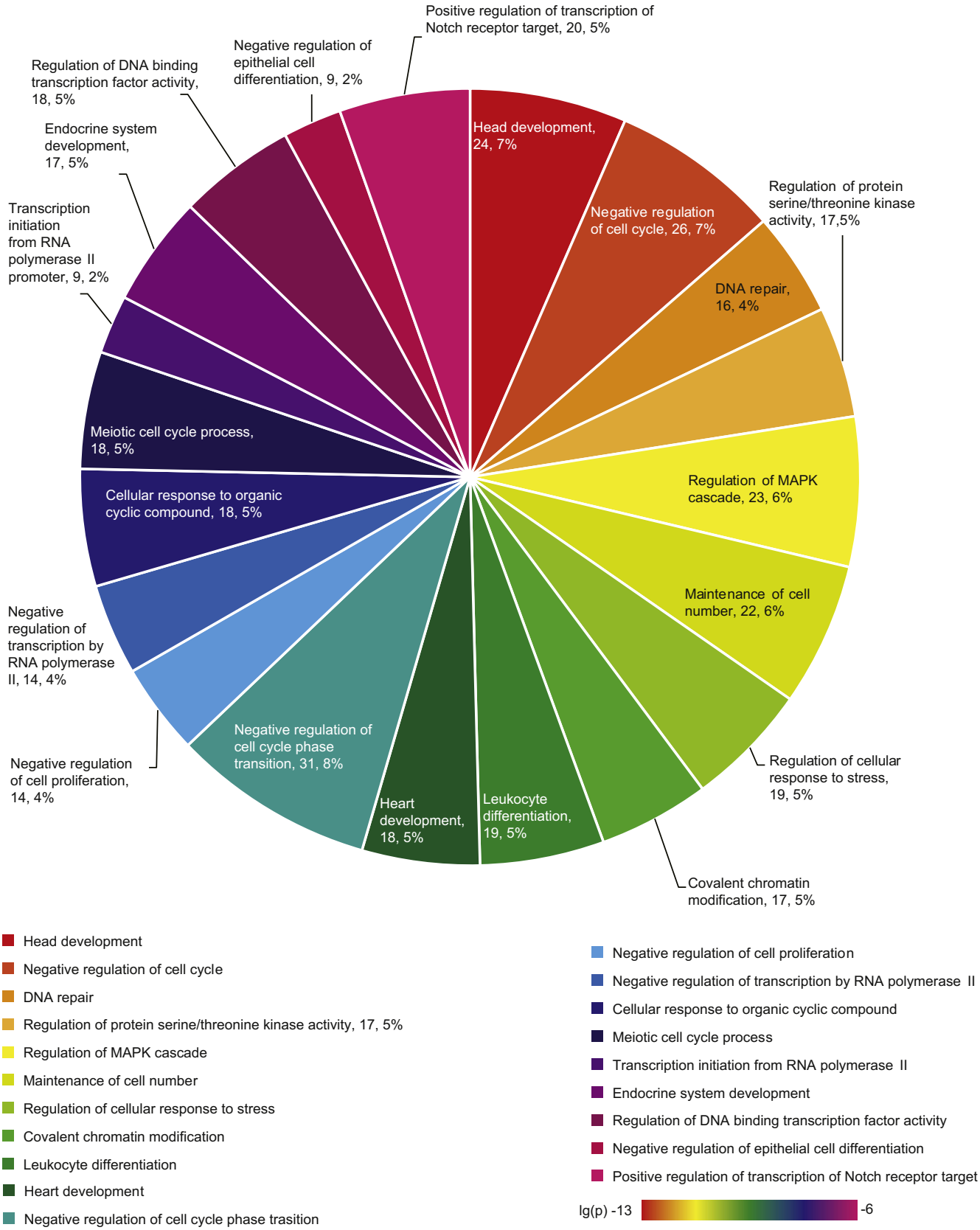

Fig. 3 Biological process analysis of 61 mutant genes.

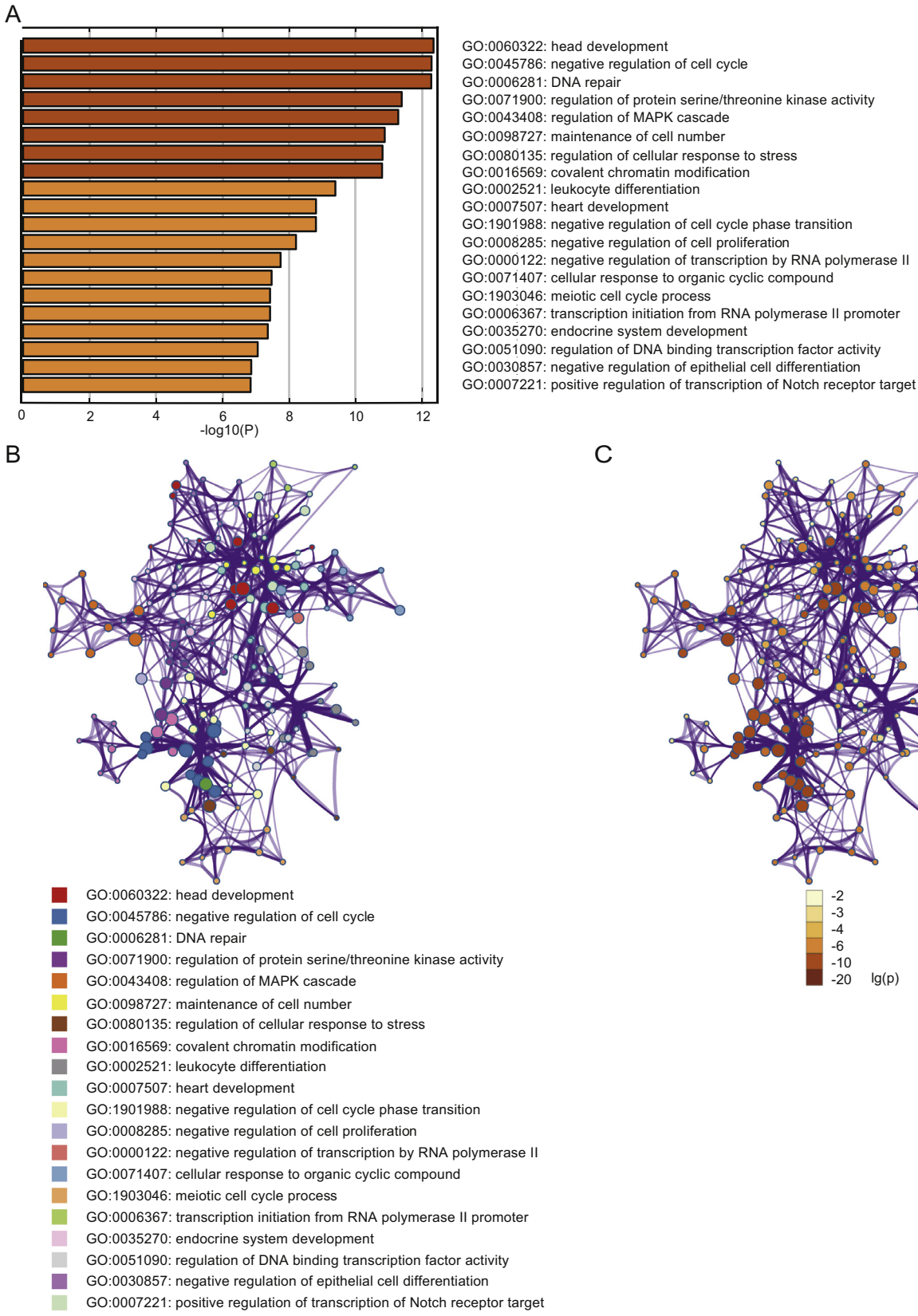

Fig. 4 Top 20 clusters with their representative enriched terms (1 per cluster) in biological processes. A, *P* value of each cluster. B, Network enrichment analysis by Metascape. Each cluster is represented by a different color, and a circle node represents each enriched term. Nodes sharing the same cluster typically are close together. C, *P* value of each term. Terms containing more genes tend to have a more significant *P* value. The smaller the *P* value, the darker the color of the node.

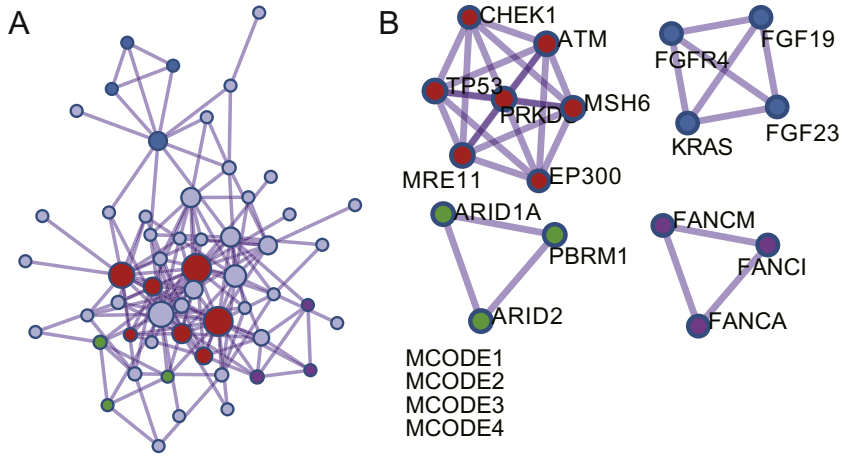

Fig. 5 Protein-protein interaction network and MCODE components identified in the gene list. A, Protein-protein interaction network. B, Four MCODE components identified in the gene list.

benign. In children and adolescents (age <18 years; n = 7), there were 1471 mutant sites. Each child/adolescent showed 210 mutations on average, with 41 (2.8%) of uncertain significance, 38 (2.6%) likely benign, and 1392 (94.6%) benign. There were 1836 mutant sites and 367 mutations per person in adults (age ≥18 years; n = 5), with 35 (1.1%) of uncertain significance, 22 (1.2%) likely benign, and 1779 (96.9%) benign. Compared with children or adolescents, adults showed more germline mutations. However, *TP53* mutations, which are deemed probably to be pathogenetic for many disorders, were not present.

3.4. GO enrichment analysis and protein-protein interaction enrichment analysis

Sixty-one mutated genes were used for GO enrichment analysis, covering biological processes, cellular components, and molecular functions, which was carried out with Metascape (http://metascape.org) [5]. As shown in Figs. 3 and 4, many biological processes, mainly brain related, head development, and MAPK, were apparent in the pathogenesis of PXA. The mutant genes were distributed on nuclear chromosomes, chromosomal regions, transferase complexes, transcription factor complexes, receptor complexes, and the cell surface (Supplementary Fig. 1). The molecular functions of the 61 genes focused on the aspects of chromosome, kinase, and protein modification. As shown in Supplementary Fig. 2, the results corresponded to their biological processes and cellular components. In total, 4 MCODEs were clustered (Fig. 5). The MCODEs are related to DNA damage, repair, modification, organization, and checkpoints.

3.5. Microsatellite instability in PXA

Because some PXAs showed mutations in DNA repair–related genes, immunostaining was used to investigate whether tumor cells showed microsatellite instability (MI). As shown in Table 1, there was positivity of MLH1, PMS2, MSH2, and MSH6 in the tumor cells, which indicated microsatellite stability. The immunohistochemical results were consistent with our NGS analysis. All the PXA cases showed fewer than nine MI sites via MI analysis. Thus, MI probably is not important in the pathogenesis of PXA.

4. Discussion

A *BRAF* mutation is a common event in CNS tumors, with a high incidence in PXA. The mutation rate in WHO grade II PXA is approximately 60% [7,8]. However, in our data, *BRAF* mutation was detected in only 38% of patients. In addition to the *BRAF* V600E mutation, Phillips identified in-frame genomic rearrangements predicted to result in *NRF1-BRAF*, constitutively active kinase fusions, in 2 anaplastic PXA tumors without *BRAF* V600E mutations [9]. It also is noteworthy that there was only 1 patient (case 14) with a *CDKN2A/B* deletion. Compared with other reports, our *CDKN2A/B* deletion rate is far lower, whereas it was present in 6 of 10 cases using comparative genomic hybridization [10] and 83% in 24 patients with PXA using the OncoScan array [11]. *CDKN2C* deletion was detected in only 1 case. We believe that this difference may be attributable to the small number of specimens in our series. On the other hand, just like the mutation rate of *EGFR* in non–small cell lung cancer, which differs by ethnicity (47% in the Asia-Pacific subgroup versus 12% in the Oceania subgroup) [12], all of the patients in our study were of Han nationality, the largest nationality in China, so the difference in both the *BRAF* V600E and *CDKN2A/B* mutation rate in our and other studies may result from different ethnicity.

To the best of our knowledge, the *KRAS* mutation was detected here for the first time in PXA. As a member of the MAPK pathway, *KRAS* alterations have been detected frequently in sporadic cancers, such as those of the colon, lung, pancreas, and the myeloid system [13], and among 505 of

1267 colorectal cancers in another series, a codon 61 mutation was detected in 19 (1.5%) [14].

Because MAPK pathway–related gene mutations, including of *KRAS*, *BRAF*, *NF1*, *CDKN2A/B/C*, were detected in all the cases in our study, and they exhibited a mutually exclusive correlation with *BRAF*, we propose that the major pathway in the pathogenesis of PXA is MAPK. Inhibition of this pathway should therefore be an effective method for treatment for most patients with PXA after surgery. Apart from the MAPK pathway, other changes such as double-strand breaks, cell-cycle arrest, DNA repair, and the PI3K-AKT pathway may be involved in the oncogenesis of PXA. The possible mechanism of PXA is illustrated in Supplementary Fig. 3.

This tumor is prevalent in children. However, germline mutation cannot explain the pathogenesis of PXA in this population. The germline mutations detected in our analysis did not include pathogenic or likely pathogenic mutations. On the contrary, more germline mutations were found in adults than in children. Moreover, *TP53* was thought to be the most frequently detected pathogenic or likely pathogenic germline mutation in 1120 patients younger than 20 years [15], which was not detected in our study.

We used data from TCGA to explore the different mutant genes and biomarkers to distinguish PXA from GBM. The *BRAF* and *FANCA* mutations and CNV of *CDKN2A/B* were evidently good biomarkers to differentiate PXA from GBM. Both *PTEN* and *EGFR* are mutated genes reported in GBM several studies [9,16-18]. However, neither mutation has been reported in our or other studies. Unfortunately, their mutation frequency is not high enough to distinguish PXA from GBM.

Supplementary data

Supplementary data to this article can be found online at https://doi.org/10.1016/j.humpath.2018.08.038.

References

[1] Kepes JJ, Rubinstein LJ, Eng LF. Pleomorphic xanthoastrocytoma: a distinctive meningocerebral glioma of young subjects with relatively favorable prognosis: a study of 12 cases. Cancer 1979;44:1839-52.
[2] Louis DN, Ohgaki H, Wiestler O, et al. World Health Organization Histological Classification of Tumours of the Central Nervous System. Lyon: International Agency for Research on Cancer; 2016.
[3] Lehman NL, Hattab EM, Mobley BC, et al. Morphological and molecular features of astroblastoma, including BRAFV600E mutations, suggest an ontological relationship to other cortical-based gliomas of children and young adults. Neuro Oncol 2017;19:31-42.
[4] Hu Z, Muller S, Qian G, et al. Human papillomavirus 16 oncoprotein regulates the translocation of beta-catenin via the activation of epidermal growth factor receptor. Cancer 2015;121:214-25.
[5] Tripathi S, Pohl MO, Zhou Y, et al. Meta- and orthogonal integration of influenza "OMICs" data defines a role for UBR4 in virus budding. Cell Host Microbe 2015;18:723-35.
[6] Ioannidis JPA. The proposal to lower *P* value thresholds to .005. JAMA 2018;319:1429-30.
[7] Dias-Santagata D, Lam Q, Vernovsky K, et al. BRAF V600E mutations are common in pleomorphic xanthoastrocytoma: diagnostic and therapeutic implications. PLoS One 2011;6:e17948.
[8] Schindler G, Capper D, Meyer J, et al. Analysis of BRAF V600E mutation in 1,320 nervous system tumors reveals high mutation frequencies in pleomorphic xanthoastrocytoma, ganglioglioma and extra-cerebellar pilocytic astrocytoma. Acta Neuropathol 2011;121:397-405.
[9] Phillips JJ, Gong H, Chen K, et al. Activating NRF1-BRAF and ATG7-RAF1 fusions in anaplastic pleomorphic xanthoastrocytoma without BRAF p.V600E mutation. Acta Neuropathol 2016;132:757-60.
[10] Weber RG, Hoischen A, Ehrler M, et al. Frequent loss of chromosome 9, homozygous CDKN2A/p14(ARF)/CDKN2B deletion and low TSC1 mRNA expression in pleomorphic xanthoastrocytomas. Oncogene 2007;26:1088-97.
[11] Vaubel RA, Caron AA, Yamada S, et al. Recurrent copy number alterations in low-grade and anaplastic pleomorphic xanthoastrocytoma with and without BRAF V600E mutation. Brain Pathol 2018;28:172-82.
[12] Midha A, Dearden S, McCormack R. EGFR mutation incidence in non–small-cell lung cancer of adenocarcinoma histology: a systematic review and global map by ethnicity (mutMapII). Am J Cancer Res 2015;5:2892-911.
[13] Bos JL. *ras* oncogenes in human cancer: a review. Cancer Res 1989;49:4682-9.
[14] Imamura Y, Lochhead P, Yamauchi M, et al. Analyses of clinicopathological, molecular, and prognostic associations of KRAS codon 61 and codon 146 mutations in colorectal cancer: cohort study and literature review. Mol Cancer 2014;13:135.
[15] Zhang J, Walsh MF, Wu G, et al. Germline mutations in predisposition genes in pediatric cancer. N Engl J Med 2015;373:2336-46.
[16] Gao J, Aksoy BA, Dogrusoz U, et al. Integrative analysis of complex cancer genomics and clinical profiles using the cBioPortal. Sci Signal 2013;6:l1.
[17] Brennan CW, Verhaak RG, McKenna A, et al. The somatic genomic landscape of glioblastoma. Cell 2013;155:462-77.
[18] Cancer Genome Atlas Research Network. Comprehensive genomic characterization defines human glioblastoma genes and core pathways. Nature 2008;455:1061-8.